JOURNAL OF CATALYSIS 121, 196–201 (1990)

Alcohol Dehydration over Model Nonporous Alumina Powder

JEANNE L. SWECKER[1] AND ABHAYA K. DATYE[2]

Department of Chemical and Nuclear Engineering, University of New Mexico, Albuquerque, New Mexico 87131

Received January 31, 1989; revised May 25, 1989

The reactivity of alumina powders obtained by evaporation of aluminum in Ar/O_2 was investigated. These alumina powders contain single crystals of transitional alumina, 5–60 nm in diameter, with a surface area of 55 m^2/gm. The reactivity of the nonporous alumina was compared with that of Kaiser A-201 γ-alumina (220 m^2/gm) for the decomposition of ethanol, 1-propanol, and *t*-butanol. The product distributions on both aluminas were similar, but the nonporous alumina was more reactive than γ-alumina per unit surface area. The activation energy for the reaction was lower on the nonporous alumina. In view of these results, it appears that transitional alumina powders prepared by the evaporation method may provide good crystalline analogs to γ-alumina. These could be used as model alumina supports since the simple geometry of the primary particles facilitates examination by high-resolution TEM.

The unique and interesting properties of γ-alumina have motivated previous attempts at synthesizing model alumina structures that can be better characterized (*1*). The transitional forms of alumina are the most common oxide supports and one possible model structure consists of thin films obtained by oxidation of aluminum metal (*2–4*). While these planar aluminas are well suited for examination by transmission electron microscopy, the low surface areas necessitate UHV environments for reactivity studies. Hence, the majority of investigations in the literature have used conventional high-surface-area γ-alumina which is porous and has irregular surfaces. The results of infrared spectroscopy have been interpreted on the basis of models which assumed that low-index facets such as (100), (110), and (111) are exposed (*5, 6*). However, since γ-alumina is poorly crystallized it is not clear if the surface is indeed composed of well-defined low-index facets. Previous attempts at imaging the surface structure of alumina have used single crystals of α-alumina (*7, 8*). Recently Iijima (*9*) reported high-resolution micrographs of single crystals of a transitional alumina that was prepared by a dry process. This method of powder preparation was pioneered by Uyeda and can be applied to the synthesis of many oxides (*10*). Although the surfaces and structures of these model aluminas have been examined, there have been no reports of their catalytic activity.

Nonporous oxide supports that have primary particles of simple geometric shape have been shown to be very useful for the study of metal structure and morphology in supported catalysts (*11*). The oxide powders of SiO_2, MgO, and TiO_2 (*12, 13*) used by us previously have bulk and surface structures similar to those observed in commercially available oxide powders. However, in the case of model alumina powder, the nonporous alumina is crystalline whereas high-surface-area γ-alumina is nearly X-ray amorphous. It is therefore important to understand the surface reactivity of these model alumina supports. In this paper we report a study of the reactivity of nonporous alumina supports whose

[1] Present address: Corning Glass Works, Wilmington, NC 28405.

[2] To whom all correspondence should be addressed.

0021-9517/90 $3.00

behavior is compared with that of commercial (Kaiser A-201) alumina. The structures of the aluminas were studied using transmission electron microscopy (TEM) and powder X-ray diffraction (XRD). The surface area and pore size distribution were determined using nitrogen adsorption at 77 K. Surface reactivity was studied using temperature-programmed desorption (TPD) of pyridine and alcohol dehydration. Experimental details are reported elsewhere (*14*).

The model alumina particles are prepared by heating pure (99.9%) aluminum in a mixture of 34% oxygen in argon gas. The aluminum is heated by means of an arc discharge. The particles of alumina are formed by direct oxidation of the metal vapor in a completely dry process unlike commercial processes which crystallize the alumina from an aqueous solution. The commercial alumina was Kaiser A-201 that had been ground to 60–80 mesh. This alumina was prepared by the flash calcination of gibbsite (Bayer hydrate) and is only 93.6% pure, containing 6% water, 0.35% sodium oxide, 0.02% iron oxide, and 0.02% silica (*15*).

XRD was performed on a Scintag diffractometer to determine the crystallinity and transitional form of the aluminas. The prominent alumina peaks seen in the Kaiser γ-alumina are also seen in the model alumina in Fig. 1. The commercial alumina is much less crystalline and is difficult to assign to just one transitional form. In contrast, the model alumina (Fig. 1b) shows sharp peaks confirming that it is crystalline and appears to be a mixture of γ- and δ-forms. The surface areas of the powders were determined by the BET method. The model alumina is nonporous with surface area of 55 m^2/g. The commercial alumina is microporous with an average pore radius of 41 Å and total pore volume of 0.46 cc/g. Its surface area is 200 m^2/g.

TEM images show that the commercial alumina (Fig. 2) consists of thin sheets 4–5 nm thick having irregular surfaces. No lattice fringes are visible in this image, con-

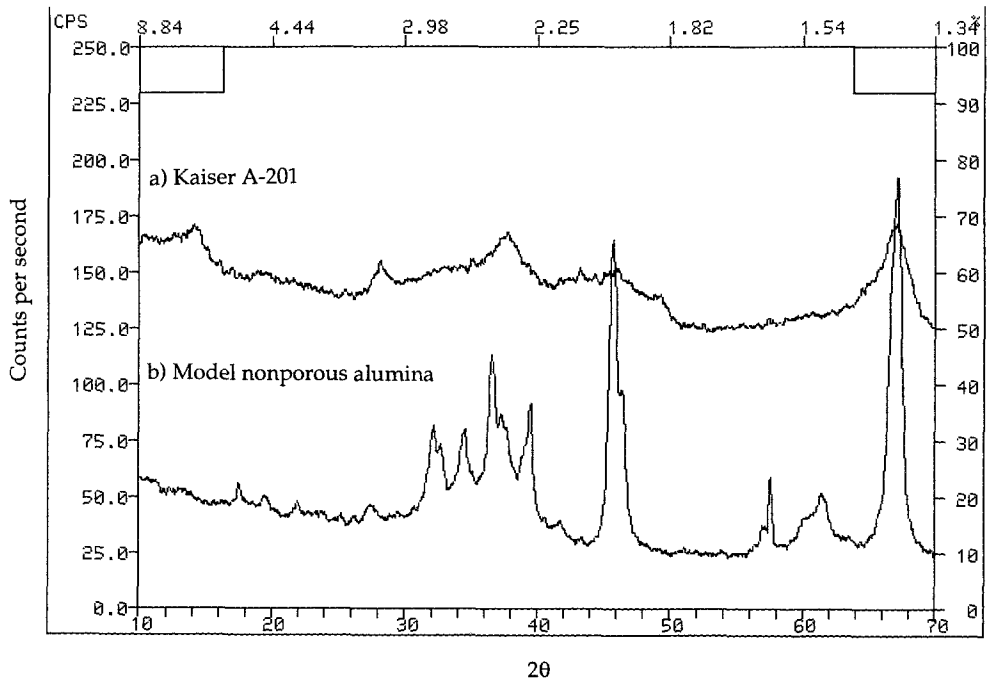

FIG. 1. XRD powder pattern of (a) Kaiser A-201 and (b) model nonporous alumina.

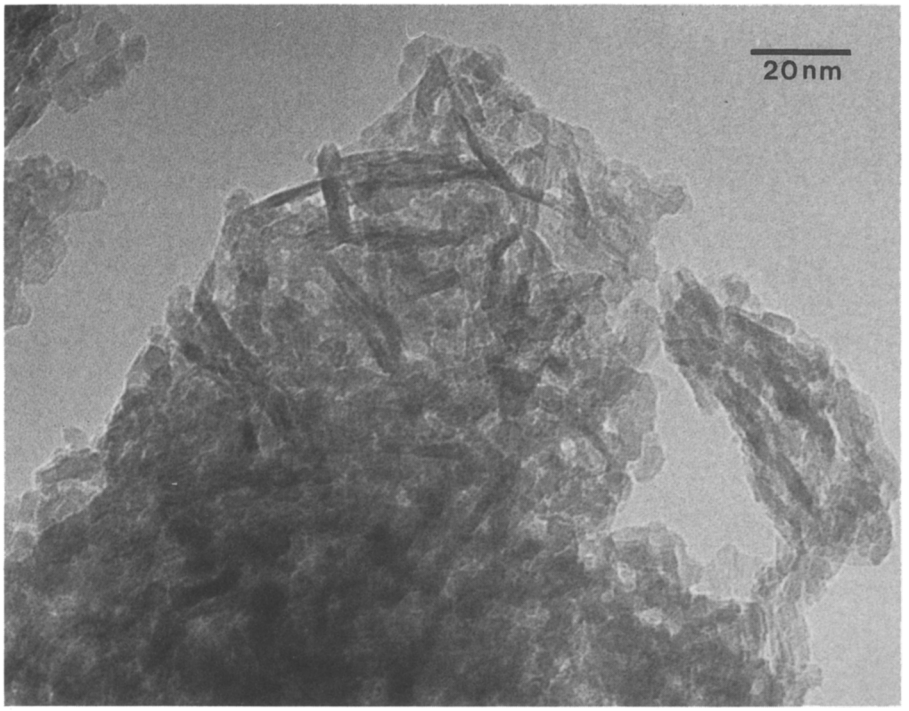

FIG. 2. Transmission electron micrograph of commercial alumina at 3.0 Å resolution (200 keV).

firming the low degree of crystallinity from the XRD measurements. The model alumina consists of nearly spherical particles of single crystals with diameters ranging from 5–60 nm (see Fig. 3a). The TEM image of the commercial alumina illustrates one of the primary problems with analysis of high-surface-area γ-alumina. The irregularly shaped particles do not exhibit well-defined facets, making it difficult to image the surface. Since the model alumina consists of nonporous spherical particles, the bulk and surface structures are readily evident in high-resolution transmission electron micrographs (HRTEM) (see Fig. 3b). HRTEM reveals surface facets and terraces similar to those reported by Iijima (*9*). Twinning of the particles can be seen and a dark line is frequently found at the facets, similar to that seen on images of electron-beam-damaged ruby reported by Bursill *et al.* (*7*). They attribute this novel contrast feature to surface potential at the polar surfaces of alumina. We have observed facets and the "black line" contrast at low and high magnification (130 kX at 200 kV and also 300 kX at 400 kV), suggesting that this feature may be inherent to the alumina surfaces.

Activity for dehydration of ethanol, 1-propanol, and *t*-butanol was measured using 30–40 mg of catalyst in a differential reactor. The catalysts were activated by heating to 400 or 600°C in flowing nitrogen. The reactant stream consisted of 14 sccm of UHP nitrogen bubbled through the alcohol at room temperature. The products were separated using a Porapak R column at 150°C for the ethanol and *t*-butanol reactions and the column was ramped between 135–185°C for the 1-propanol reaction. Analysis was performed with a thermal conductivity detector (TCD) using helium as a carrier gas. The peak areas were corrected for variations in TCD sensitivities (*16*) and the nitrogen peak was used as an

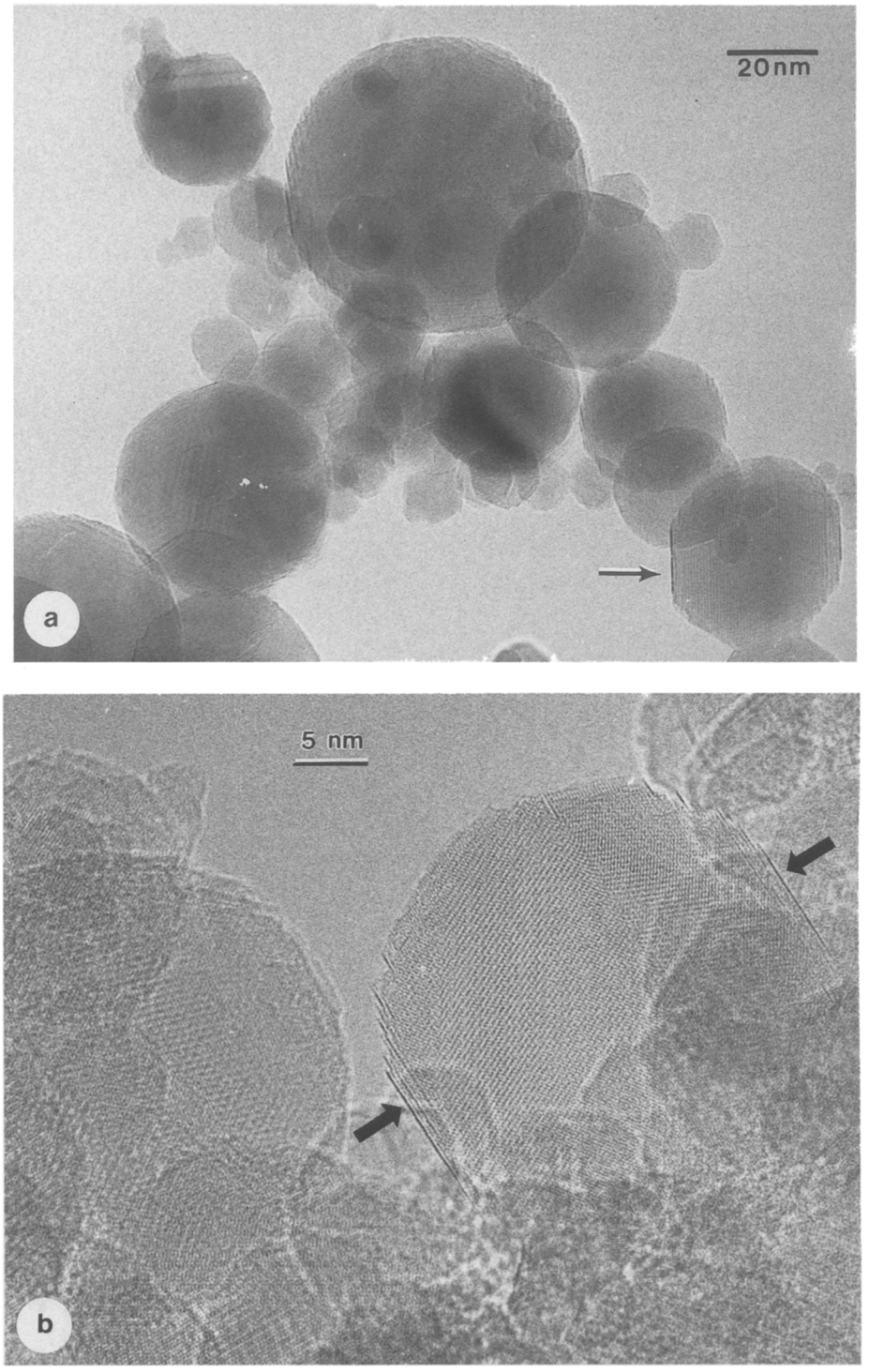

FIG. 3. Transmission electron micrographs of model alumina (a) at 3.0 Å resolution (200 keV) and (b) at 1.7 Å resolution (400 keV). Note the "black line" contrast at surface facets.

TABLE 1

Activation Energies[a] for Alcohol Dehydration

Alcohol	Sample	Olefin	Ether	S^b
Ethanol	A-201	134	95	0.13
	Model	105	82	0.32
1-Propanol	A-201	134	72	1.24
	Model	115	62	2.27
t-Butanol	A-201	114	—	—
	Model	81	—	—

[a] Activation energies in kJ/mol.

[b] S represents the molar ratio of olefin to ether in the products at a reaction temperature of 300°C.

internal standard. Reaction rates were based on the moles of product formed per second per square meter of catalyst surface area. The reactor effluent was analyzed after 15 min on stream. The catalyst activity did not decay with time and hence data represent the steady-state activity of the catalyst. Ethanol dehydration produced diethyl ether, ethylene, water, and a small amount of acetaldehyde at $T > 300$°C. The molar ratio of olefin to ether at 300°C is indicated as the selectivity S in Table 1. The formation of ether occurs via a bimolecular reaction and is therefore favored when the surface coverage of reactants is high. Hence, while ether was the major product from ethanol in the flow reactor, ethylene was the only product detected in the temperature-programmed reaction experiments performed under vacuum. Similarly, propylene was the major product from 1-propanol in the flow reactor due to the lower vapor pressure of propanol. *t*-Butanol formed only isobutylene and water due to the steric hinderance of the methyl groups. The product distributions on the model and commercial aluminas were similar, as seen in Table 1.

An Arrhenius plot for the formation of isobutylene from *t*-butanol is shown in Fig. 4 and is representative of the data obtained from the other alcohols. The model alumina had lower activation energies, calculated from Arrhenius plots, for all reactions. The differences ranged from 15 to 38 kJ/mol for olefin formation and 7 to 13 kJ/mol for ether. We suspect that impurities such as Na may have poisoned some reaction sites of the commercial alumina, resulting in higher activation energies. All of the activation energies, however, fall within the range of data reported in the literature (*18, 19*). Table 1 lists activation energies as determined from least-squares analysis of Arrhenius plots. All of the plots show excellent linearity for conversions up to 40%. No change in product distribution or activation energy was found for the aluminas activated at substantially different temperatures (400–600°C). Since water is a product of the dehydration reaction it could easily have rehydroxylated the alumina surface.

Although the model alumina is composed of single-crystal particles and is thus more ordered than the nearly amorphous A-201 alumina, both show similar catalytic properties (*14*). When reaction rates are based on surface areas, the model alumina is always more reactive (see Fig. 4). Some of the differences in reactivity seen between

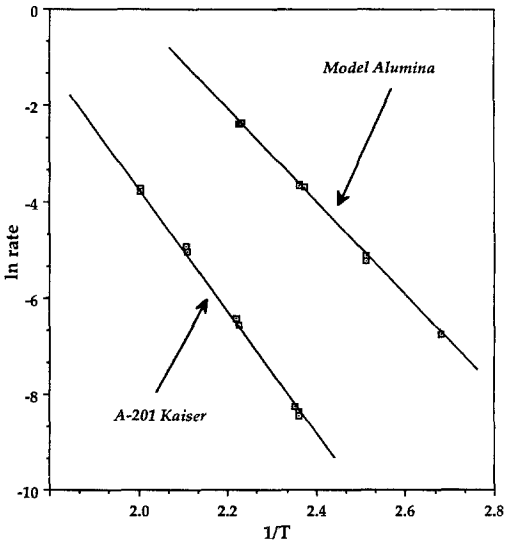

FIG. 4. Arrhenius plot for production of isobutylene from *t*-butanol over model and commercial aluminas. The rate of reaction is expressed as moles per second per square meter.

the nonporous and high-surface-area aluminas may be caused by diffusion limitations. However, it should be noted that the model alumina which is nonporous exhibits lower activation energies, especially for *t*-butanol dehydration. Knozinger has suggested that multiple vacancies may be required for alcohol dehydration (*20*). These may be more prevalent in the terraces and facets of the model alumina than on the irregular surface of the commercial alumina. Additionally, the commercial alumina contains Na which has been shown to poison acid sites of alumina (*21*).

In conclusion, the aluminas showed similar activity for alcohol dehydration even though their bulk structures were markedly different. It appears from these preliminary studies that the bulk structure may have little effect on the active sites in these aluminas at least for those sites involved in alcohol dehydration. Planar models for γ-alumina used previously consisted of microcrystalline domains bounded by disordered regions (*4*). It is not known from those studies whether the active sites lie within the crystalline or the disordered regions. By using nonporous crystalline alumina, it may be possible to study the role of bulk defects on alumina reactivity. Our results show that the nonporous aluminum oxide appears to be a good model for high-surface-area γ-alumina.

ACKNOWLEDGMENTS

This research was supported in part by a grant from the National Science Foundation (CBT-8707693). Partial funding from Associated Western Universities via a thesis grant (JS) is also acknowledged. We are grateful to Dr. D. Wayne Goodman for his help and encouragement in this research. The electron microscopy was performed at the microbeam analysis facility at the department of Geology, University of New Mexico. The high-resolution electron microscopy was performed with the assistance of Professor David J. Smith at the NSF facility for HREM at Arizona State University supported by Grant DMR-8611609.

REFERENCES

1. Cocke, D. L., Johnson, E. D., and Merrill, R. P., *Catal. Rev. -Sci. Eng.* **26,** 163 (1984).
2. Chen, J. J., and Ruckenstein, E., *J. Phys. Chem.* **85,** 1606 (1981).
3. Bischke, S. D., and Goodman, D. W., *Surf. Sci.* **150,** 351 (1985).
4. Czanderna, K. K., Morrissey, K. J., Carter, C. B., and Merrill, R. P., *J. Catal.* **89,** 182 (1984).
5. Knozinger, H., and Ratnasamy, P., *Catal. Rev. Sci. Eng.* **17,** 31 (1978).
6. Peri, J. B., *J. Phys. Chem.* **69,** 220 (1966).
7. Bursill, L. A., Lin, P. J., and Smith, D. J., *Ultramicroscopy* **23,** 223 (1987).
8. Hsu, T. and Kim, Y., presented at workshop on "Surfaces and Surface Reactions," organized by Arizona State University, Wickenburg, AZ, Jan. 1989, to be published.
9. Iijima, S., *Japan. J. Appl. Phys.* **23,** L347 (1984).
10. Uyeda, R., *J. Cryst. Growth* 24/25, 69 (1974).
11. Datye, A. K., and Long, N. J., *Ultramicroscopy* **25,** 203 (1988).
12. Datye, A. K., Logan, A. D., and Long, N. J., *J. Catal.* **109,** 76 (1988).
13. Logan, A. D., Branschweig, E. J., Datye, A. K., and Smith, D. J., *Langmuir* **4,** 827 (1988).
14. Swecker, J. L., M. S. thesis, Dept. of Chemical and Nuclear Engineering, University of New Mexico, Albuquerque, NM, 1989.
15. Product data, Activated Alumina A-201, La Roche Chemicals, 1987.
16. Messner, A. E., Rosie, D. M., and Argabright, P. A., *Anal. Chem.* **31,** 230 (1959).
17. Vit, Z., *Collect. Czech. Chem. Commun.* **50,** 1268 (1985).
18. Yue, P. L., and Olaofe, O., *Chem. Eng. Res. Des.* **62,** 81 (1984).
19. Knozinger, H., Buhl, H., and Kochloefl, K., *J. Catal.* **24,** 57 (1972).
20. Knozinger, H., *in* "Catalysis by Acids and Bases" (B. Imelik *et al.*, Eds.), p. 111. Elsevier Science Publishers BV, Amsterdam, 1985.
21. Luy, J. C., and Parera, J. M., *Appl. Catal.* **26,** 295 (1986).